

## Colorimetric and fluorescent determination of sulfide and sulfite with kinetic discrimination

Xiaoliang Pei,<sup>a</sup> Haiyu Tian,<sup>a</sup> Weibing Zhang,<sup>a\*</sup> Albert M. Brouwer<sup>b</sup> and Junhong Qian<sup>a\*</sup>

<sup>a</sup>Shanghai Key Laboratory of Functional Materials Chemistry, School of Chemistry and Molecular Engineering, East China University of Science and Technology, Shanghai 200237, China. e-mail: junhongqian@ecust.edu.cn, weibingzhang@ecust.edu.cn

<sup>b</sup>Van 't Hoff Institute for Molecular Sciences, Faculty of Science, University of Amsterdam, PO Box 94157, 1090 GD Amsterdam, The Netherlands. E-mail: a.m.brouwer@uva.nl

### Supporting Information

#### Contents

Experimental-----	2
NMR and ESI spectra of <i>m</i> -PSP and <i>p</i> -PSP-----	4
Dynamic reaction curves of <i>m</i> -PSP and <i>p</i> -PSP -----	6
NMR and ESI spectra of <i>m</i> -PSP-SO <sub>3</sub> H-----	7
NMR of the reaction product between <i>m</i> -PSP and sulfide-----	8
Time-dependent fluorescence spectra of <i>p</i> -PSP in the presence of sulfite/sulfide-----	9
Time-dependent spectra of <b>TSP2</b> in the presence of sulfite-----	10
Time-dependent spectra of <b>m6</b> in the presence of sulfite/sulfide-----	11
The absorption and emission spectra of <i>m</i> -PSP coexisted with various agents-----	12
The visible and fluorescence colors of <i>m</i> -PSP coexisted with various agents -----	13
Quantitative curves with error bars-----	14
The absorption and emission spectra of <i>p</i> -PSP coexisted with various agents-----	15
Living cell imaging of <i>p</i> -PSP-----	16
Computed molecular structures -----	17
Energies and excitation energies of selected conformers-----	18
Frontier orbitals of the lowest-energy conformer of <i>m</i> -PSP-SH-----	20

## Experimental Section

### Materials and Reagents

All chemicals (analytical grade) were purchased from Aladdin Corporation and used without further purification. Ultra-pure water was prepared through a Sartorius Arium611DI system. Phosphate salts were used to keep a stable pH and ion strength in detection systems.

Absorption spectra were carried out in an Evolution 220 UV-Visible spectrophotometer (Thermo Scientific). Fluorescence spectra were measured with a Lumina Fluorescence Spectrometer (Thermo Scientific). NMR spectra were recorded on a Bruker AV-400 spectrometer (400 MHz). Mass spectra were performed with a MA 1212 Instrument using standard condition (ESI, 70 eV).

### Computational methods

Geometry optimizations were performed using the B3LYP hybrid density functional method with the 6-31G(d) basis set using the Polarizable Continuum Model for water as implemented in Gaussian09. The energy minima were characterized as such by calculation of the vibrational frequencies. Vertical excitation energies and oscillator strengths were computed at the optimized geometries using three approaches: (1) B3LYP, (2) CAM-B3LYP and (3) PBE0 in all cases using the 6-31G+(d) basis set.

### Absorbance and fluorescence titration

Stock solutions of  $3 \times 10^{-2}$  M *m*-PSP/ *p*-PSP in DMF, 10 mM Na<sub>2</sub>S in phosphate buffer solution (PBS) and 10 mM Na<sub>2</sub>SO<sub>3</sub> in PBS (20 mM, pH 7.4) were prepared in advance. 10  $\mu$ L of *m*-PSP/ *p*-PSP stock solution was added to 3 mL of PBS solution to make [dye] = 10  $\mu$ M. 0 ~ 50  $\mu$ L of sulfite or sulfide stock solution were added to the dye-PBS solution to obtain appropriate concentrations of sulfite or sulfide. The quantum yields were determined with Coumarin 153 as the reference.

### HPLC traces

HPLC analysis were carried out on an Elliot 1203 system with a Zobax C18 reversed-phase column (4.6 mm $\times$ 10 cm). The mobile phases were degassed with an ultrasonic apparatus for 10 min. Mobile phase: A: water, B: acetonitrile; gradient elution: 3–15 min 5–95% B, 16–20 min 95–5% B; Isocratic elution: 0–3 5% B, and 15–16 min 95% B. Injection volume: 50  $\mu$ L; flow rate: 1.0 mL/min; detection wavelength: isosbestic point 450 nm.

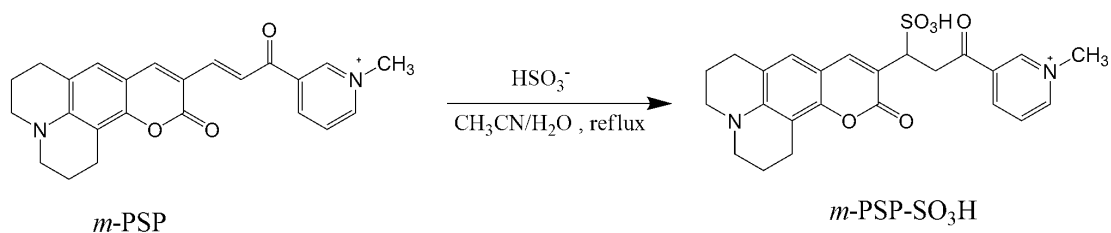
### Living cell culture and fluorescence imaging

L929 cells were cultured in Dulbecco's modified Eagle's medium (DMEM) supplemented with 10% fetal bovine serum (FBS) at 37 °C and under 5% CO<sub>2</sub> in a CO<sub>2</sub> incubator. The cells were washed with phosphate buffer solution (PBS, 20 mM, pH 7.4) and pre-incubated with 100  $\mu$ M Na<sub>2</sub>S or Na<sub>2</sub>SO<sub>3</sub>, then incubated with *m*-PSP (10  $\mu$ M) in DMEM for 120 min (Na<sub>2</sub>S) or 30 min (Na<sub>2</sub>SO<sub>3</sub>) at 37 °C followed by washing 3 times with PBS. For the control experiment, the cells were only incubated with 10  $\mu$ M of *m*-PSP for 120 min. Cell imaging was carried out after washing cells with PBS. Emission was collected at green channel.

### Determination of the detection limit

The detection limit (LOD) was obtained by  $3S_b/k$ , where  $S_b$  is the standard deviation of the blank measurements of 10 times, and  $k$  is the slope of the fitted line.

**Synthesis of *m*-PSP-SO<sub>3</sub>H:** A solution of 32.56 mg Na<sub>2</sub>SO<sub>3</sub> in 2 mL H<sub>2</sub>O was added dropwise to 10 mL EtOH containing 20 mg of *m*-PSP. The mixture was refluxed for 12 h to give *m*-PSP-SO<sub>3</sub>H as a brick-red solid (yield: 72%). <sup>1</sup>H-NMR (400 MHz, DMSO-*d*<sub>6</sub>) δ (ppm): 9.53 (s, 1 H), 9.11 (d, 1 H, *J* = 5.3 Hz), 8.97 (d, 1 H, *J* = 8.5 Hz), 8.24 (m, 1 H), 7.77 (s, 1 H), 6.91 (s, 1 H), 6.07 (m, 1 H), 5.33 (m, 1 H), 4.49 (m, 1 H), 4.41 (s, 3 H), 2.73 (m, 12 H); <sup>13</sup>C NMR (400MHz, DMSO-*d*<sub>6</sub>) δ (ppm): 185.0, 160.4, 152.2, 148.8, 148.3, 144.0, 143.6, 134.9, 128.3, 127.3, 126.2, 120.2, 118.8, 111.3, 105.6, 56.5, 50.2, 49.7, 29.5, 27.2, 21.0, 20.0, 19.0; HR-MS *m/z*: 469.1429 (M); calculated molecular weight of C<sub>24</sub>H<sub>26</sub>N<sub>2</sub>O<sub>6</sub>S<sup>+</sup>: 469.1433 for (M).



**Scheme 1** The synthesis of the addition product *m*-PSP-SO<sub>3</sub>H.

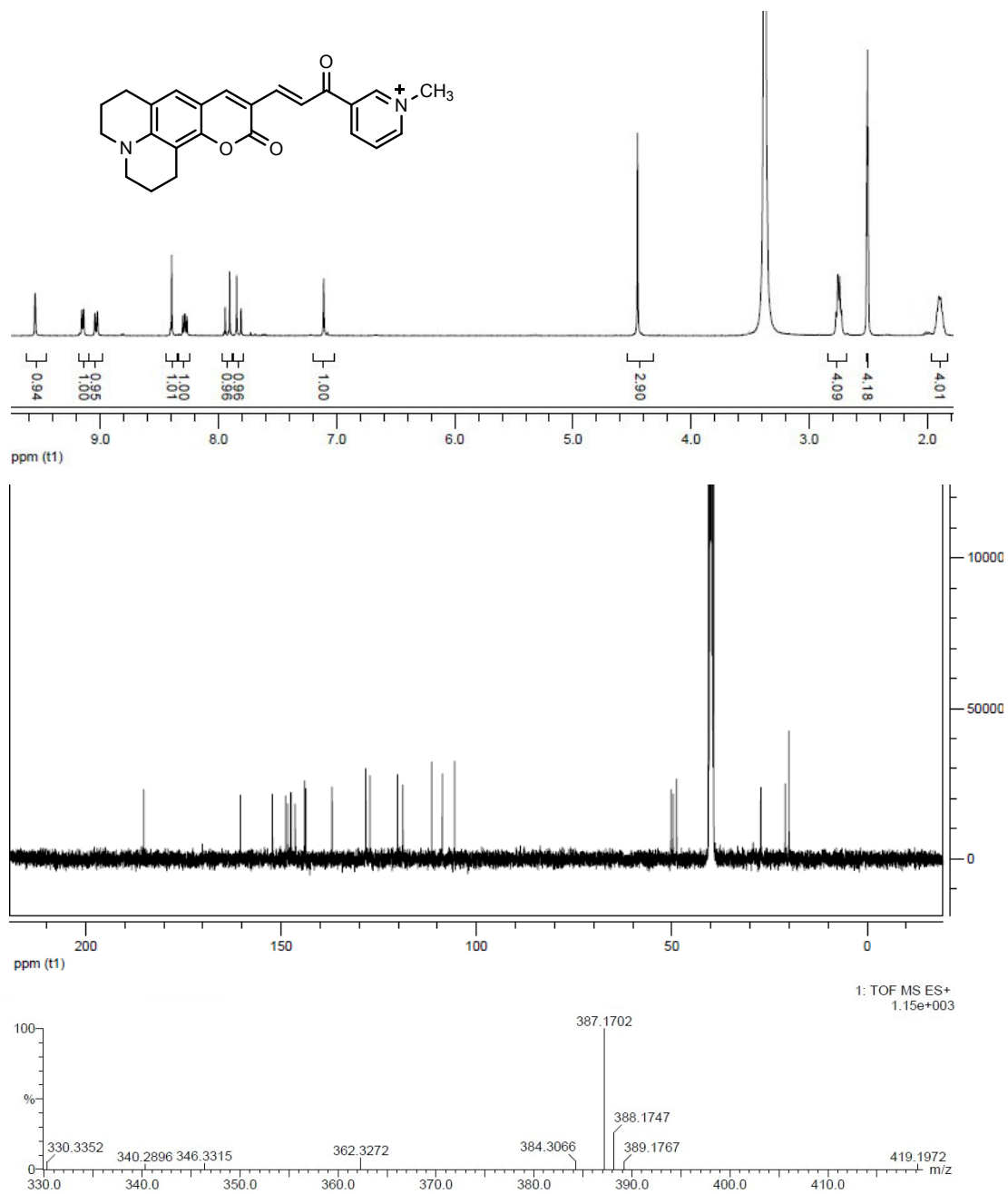


**Fig. S1** <sup>1</sup>H NMR, <sup>13</sup>C NMR and ESI spectra of *m*-PSP.

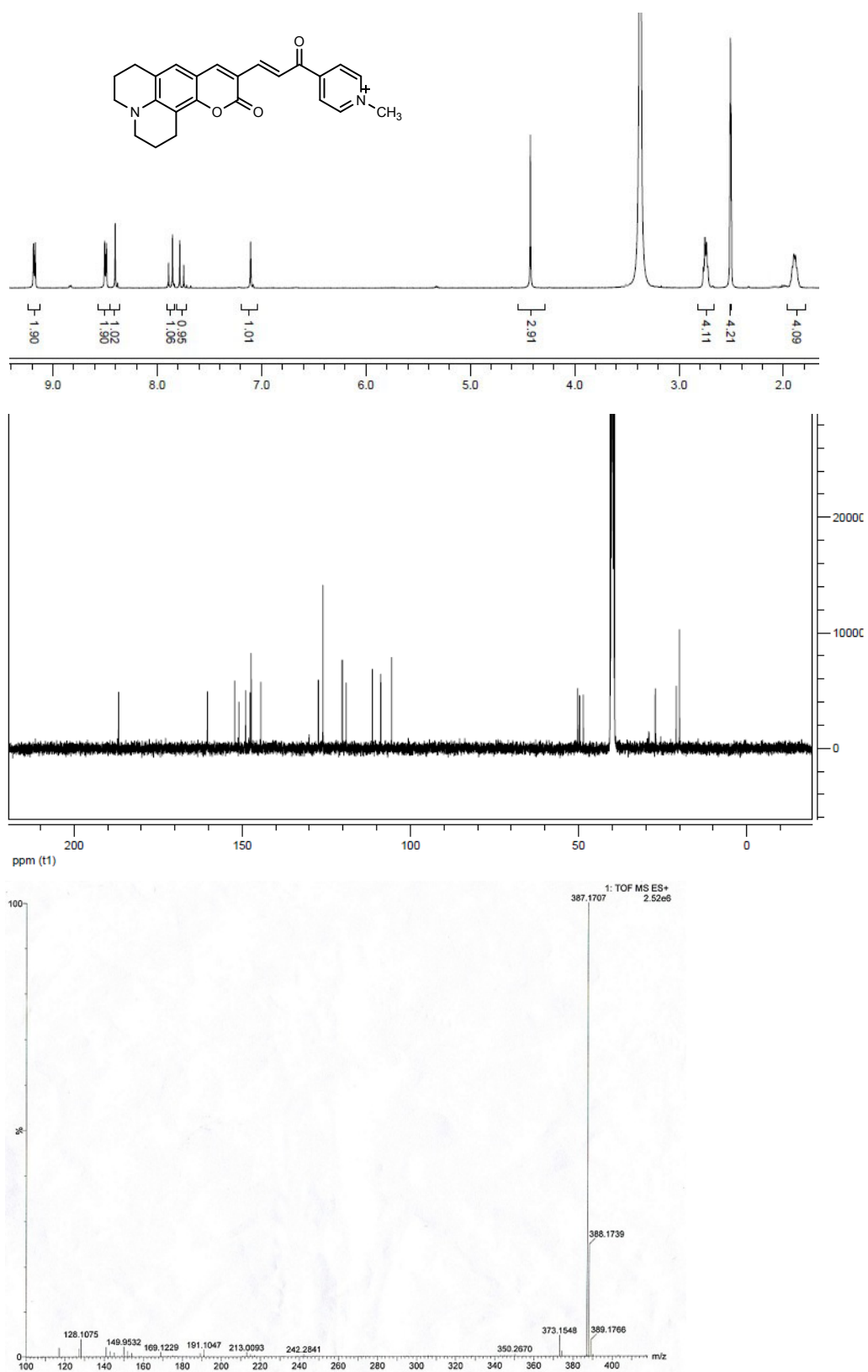
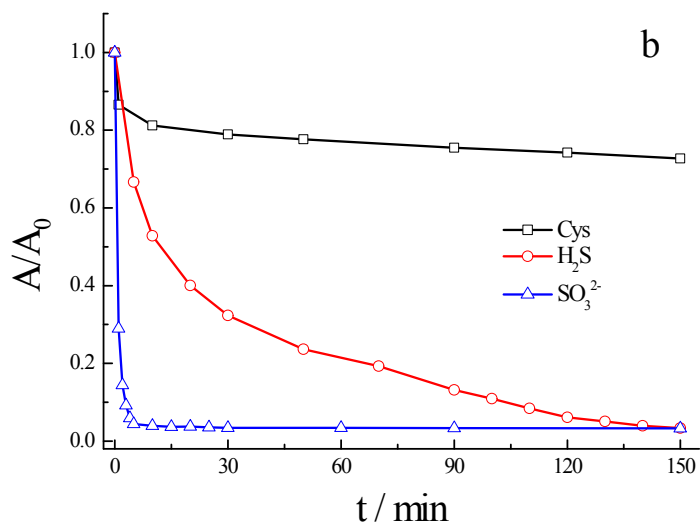
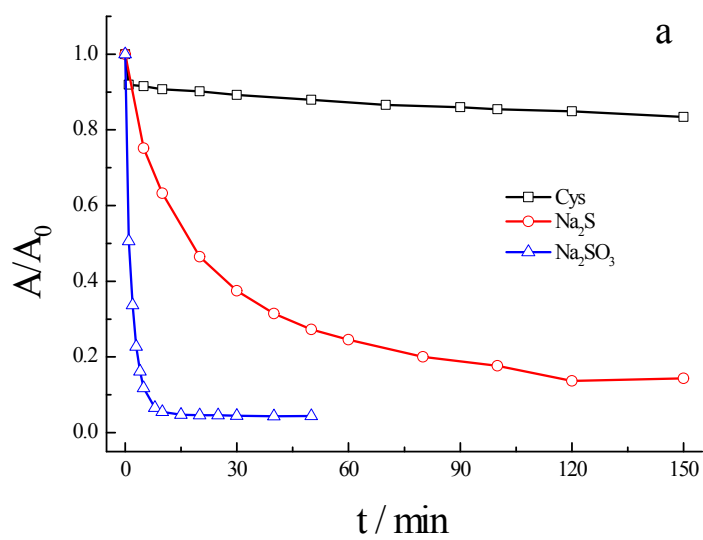
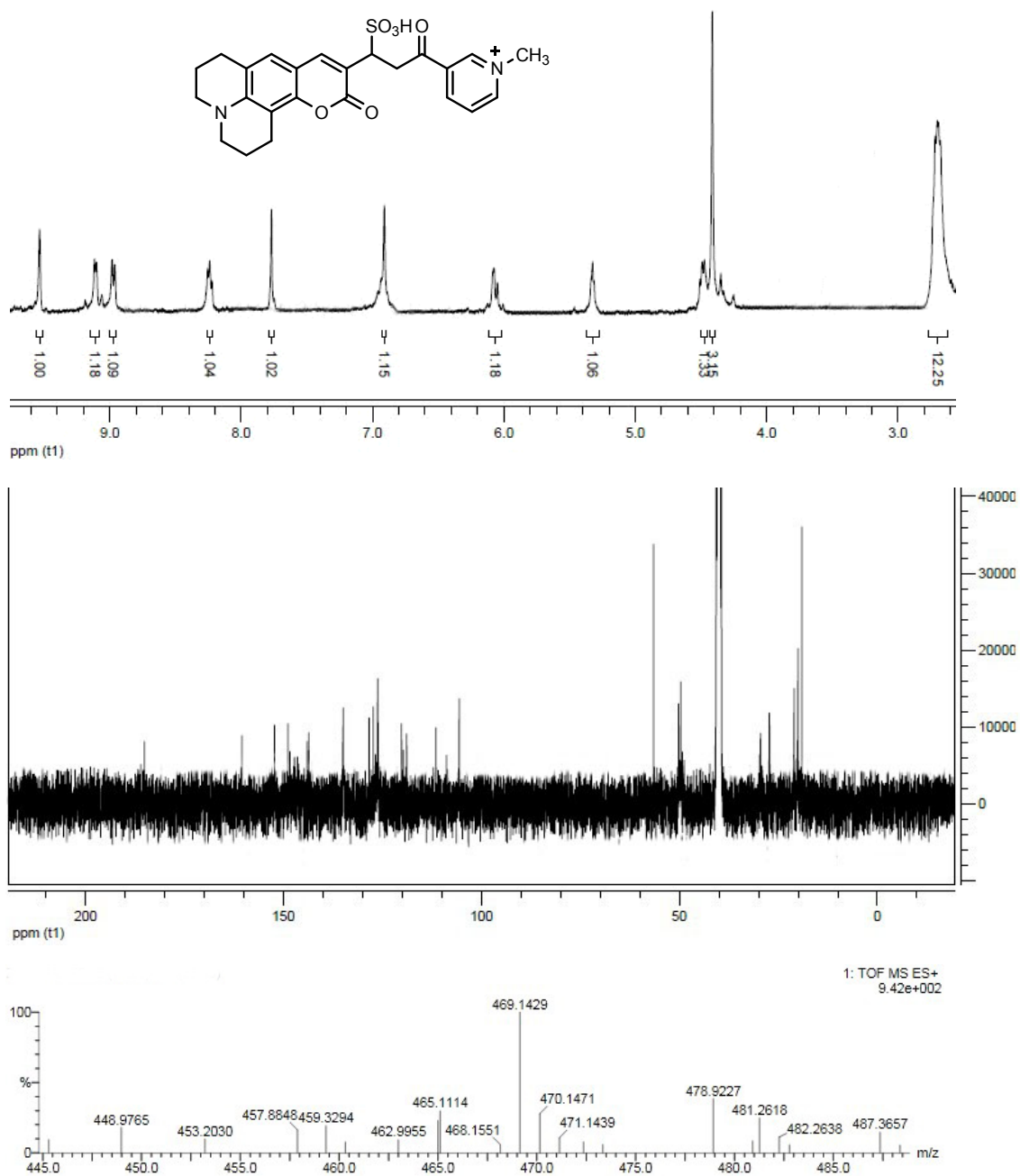


Fig. S2 <sup>1</sup>H NMR, <sup>13</sup>C NMR and ESI spectra of *p*-PSP.



**Fig. S3** The  $A_t/A_0$  plots of *m*-PSP (a, 10  $\mu\text{M}$ ) and *p*-PSP (b, 10  $\mu\text{M}$ ) as a function of time in the presence of 50 equiv of sulfite, sulfide and Cys in PBS.  $A_t$  and  $A_0$  are the absorbance at 529 nm at  $t$  and 0 time, respectively. 20 mM PBS, pH 7.4, 25°C.



**Fig. S4** <sup>1</sup>H NMR, <sup>13</sup>C NMR and ESI spectra of the addition product *m*-PSP-SO<sub>3</sub>H.

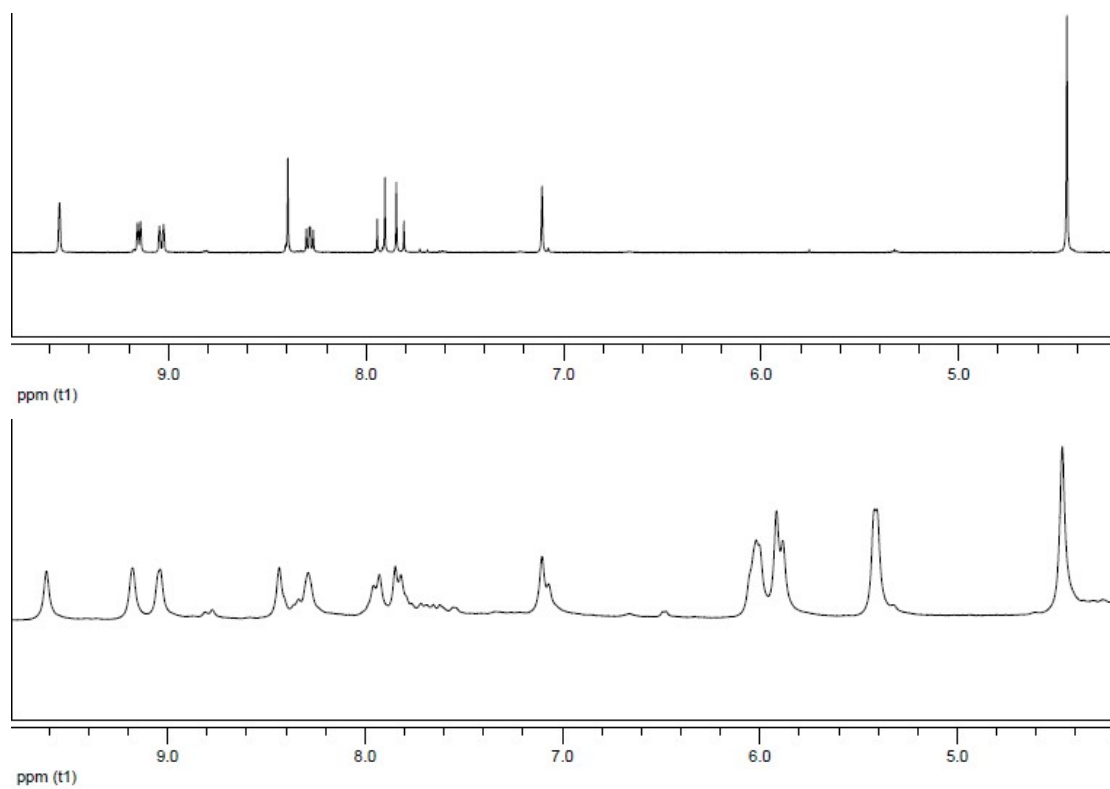


**Fig. S5** Partial  $^1\text{H}$  NMR spectra of *m*-PSP (top) and the mixture of *m*-PSP and  $\text{Na}_2\text{S}$  (bottom, 12 h) in  $\text{DMSO-}d_6$ .

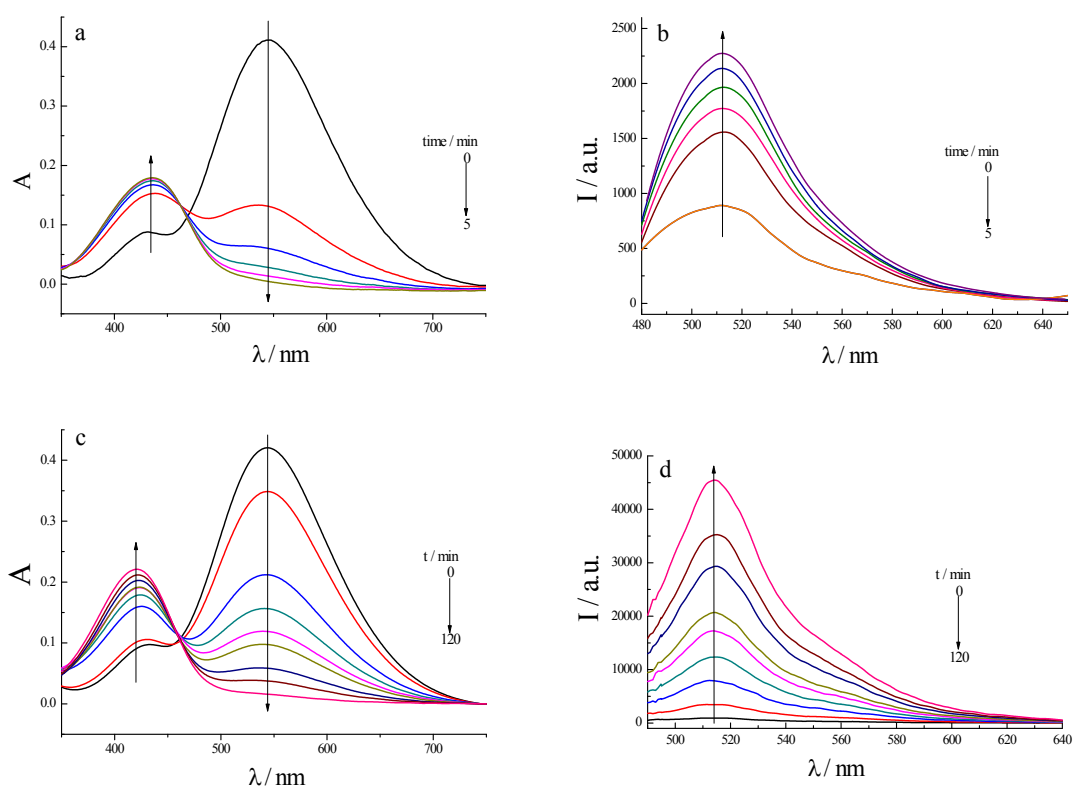


**Fig. S6** Time-dependent absorption (a, c) and emission spectra (b, d) of *p*-PSP (10 μM) in the presence of 0.5 mM of sulfite (a, b) or sulfide (c, d) in PBS (20 mM) system. pH = 7.4, 25 °C, excited at the isosbestic point ( $\lambda_{\text{ex}} = 460 \text{ nm}$ ).

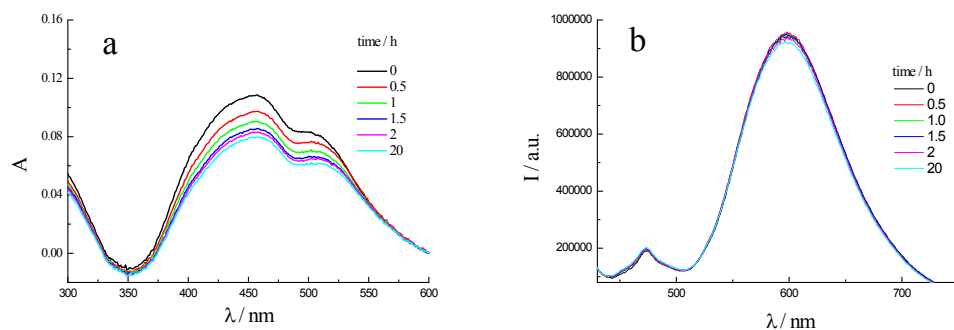


**Fig. S7** Time-dependent absorption (a) and emission spectra (b) of **TSP2** (10 μM) in the presence of 50 equiv of sulfite in PBS. 20 mM PBS, pH 7.4, [sulfite] = 500 μM,  $\lambda_{\text{ex}}$  = 410 nm, 25°C.

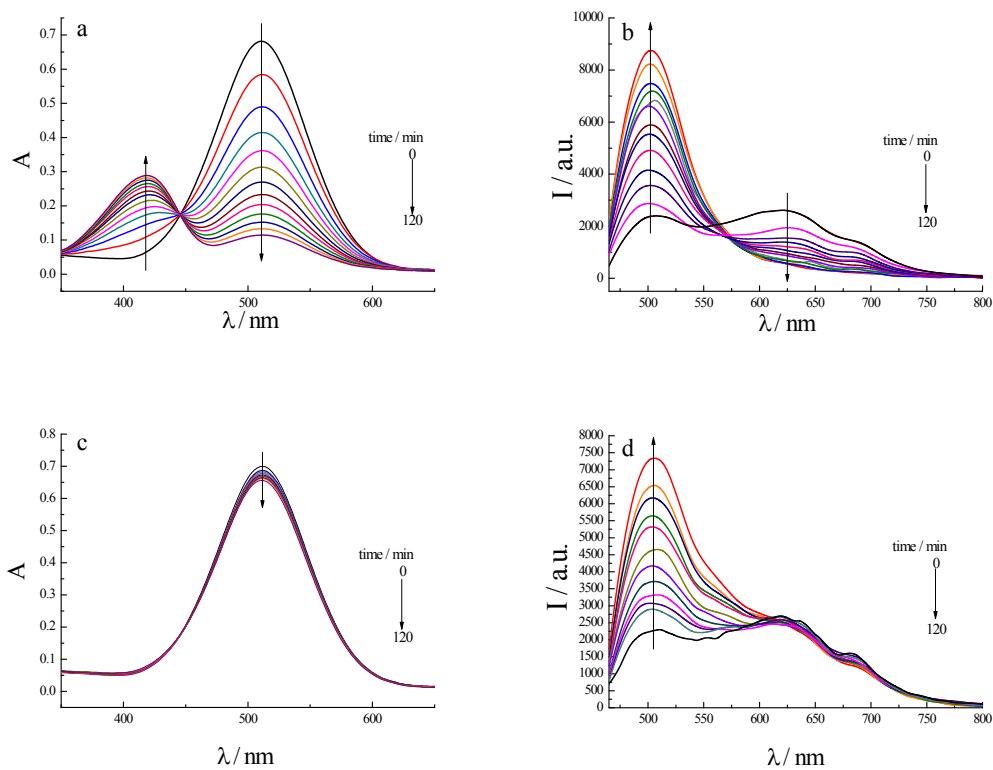


**Fig. S8** Time-dependent absorption (a, c) and emission spectra (b, d) of **m6** (10  $\mu\text{M}$ ) in the presence of 0.5 mM of sulfite (a, b) and sulfide (c, d) in 3:7 DMF-PBS (20 mM PBS) system. pH 7.4, 25  $^{\circ}\text{C}$ , excited at the isosbestic point ( $\lambda_{\text{ex}} = 445 \text{ nm}$ ).

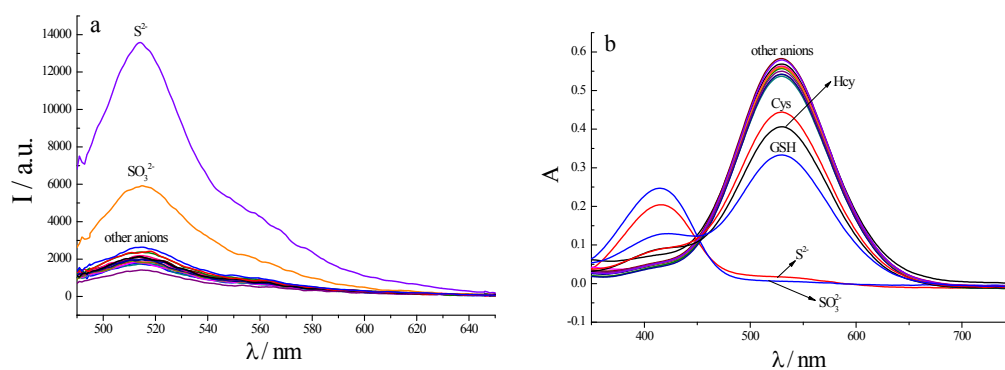


**Fig. S9** The emission (a, recorded 10 min after addition of the reagent) and absorption (b, monitored 2 h after addition of the reagent) spectra of *m*-PSP (10 μM) in the presence of 50 equiv. of various additives, including  $F^-$ ,  $Cl^-$ ,  $Br^-$ ,  $AcO^-$ ,  $HCO_3^-$ ,  $CN^-$ ,  $SCN^-$ ,  $NO_2^-$ ,  $NO_3^-$ ,  $PO_4^{3-}$ ,  $SO_4^{2-}$ ,  $S_2O_3^{2-}$ , Cys, Hcy, GSH,  $Na_2S$  and  $Na_2SO_3$  in PBS, 20 mM, pH 7.4,  $\lambda_{ex} = 450$  nm.

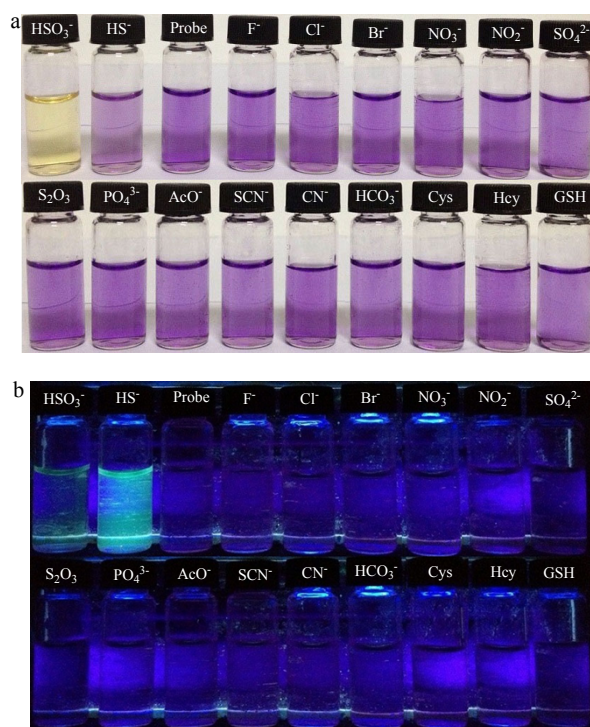


**Fig. S10** Visible (a, in natural light ~10 min after addition of the reagent) and fluorescence photos (b, on excitation at 365 nm using UV lamp ~2 h after addition of the reagent) of *m*-PSP (10 μM) with various additives (50 equiv.) in PBS (20 mM, pH 7.4).

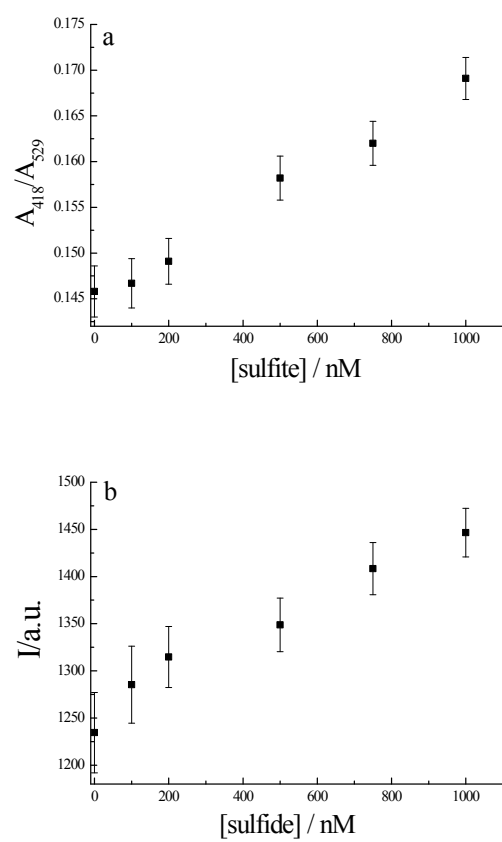


**Fig. S11** The absorbance ratio at 418 nm and 529 nm ( $A_{418}/A_{529}$ , a, sulfite) and fluorescence intensity (b, sulfide) curves for the nanomolar range, with error bars that display  $\pm 3$  standard deviations.

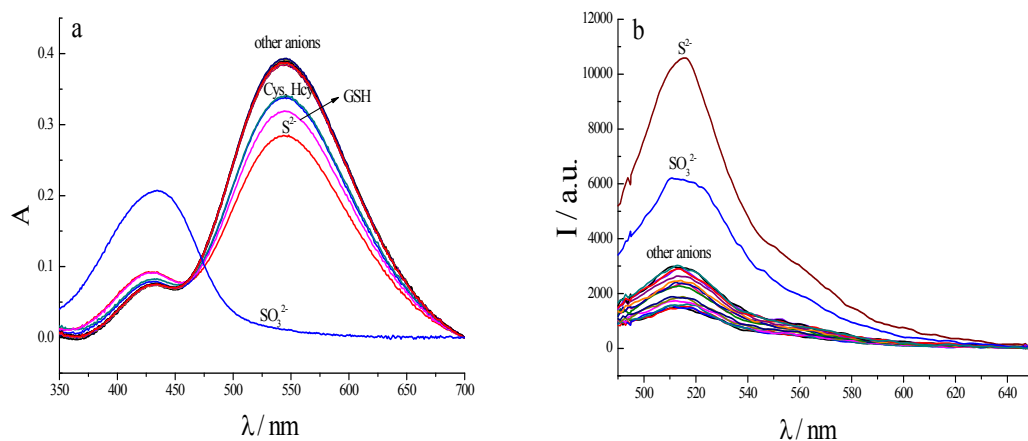


**Fig. S12** The absorption (a) and emission spectra (b) of *p*-PSP (10  $\mu$ M) in the presence of 50 equiv. of various agents, including  $F^-$ ,  $Cl^-$ ,  $Br^-$ ,  $AcO^-$ ,  $HCO_3^-$ ,  $CN^-$ ,  $SCN^-$ ,  $NO_2^-$ ,  $NO_3^-$ ,  $PO_4^{3-}$ ,  $SO_4^{2-}$ ,  $S_2O_3^{2-}$ , Cys, Hcy, GSH,  $Na_2S$  and  $Na_2SO_3$  in 20 mM PBS, pH 7.4,  $\lambda_{ex} = 460$  nm, tested 5 min after addition of the reagent.

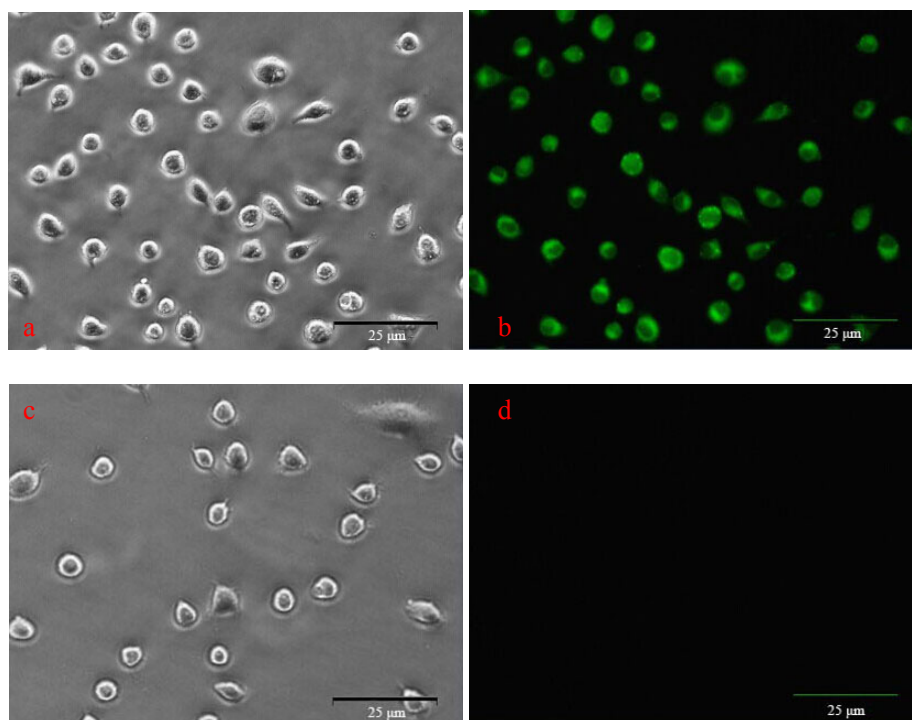


**Fig. S13** Bright-field (a, c) and fluorescence (b, d) images of living L929 cells incubated with 10  $\mu\text{M}$  *p*-PSP for 30 min. (a, b) co-incubation of 500  $\mu\text{M}$   $\text{Na}_2\text{SO}_3$  and (c, d) without any other additives.

## Computational results

The optimized geometries of relevant structures were calculated at the B3LYP/6-31G(d) level using the Polarizable Continuum Model (PCM) for water. For the probe molecules and adducts, selected structures are shown in Figure S11, and energies and excitation energies in Table S1.

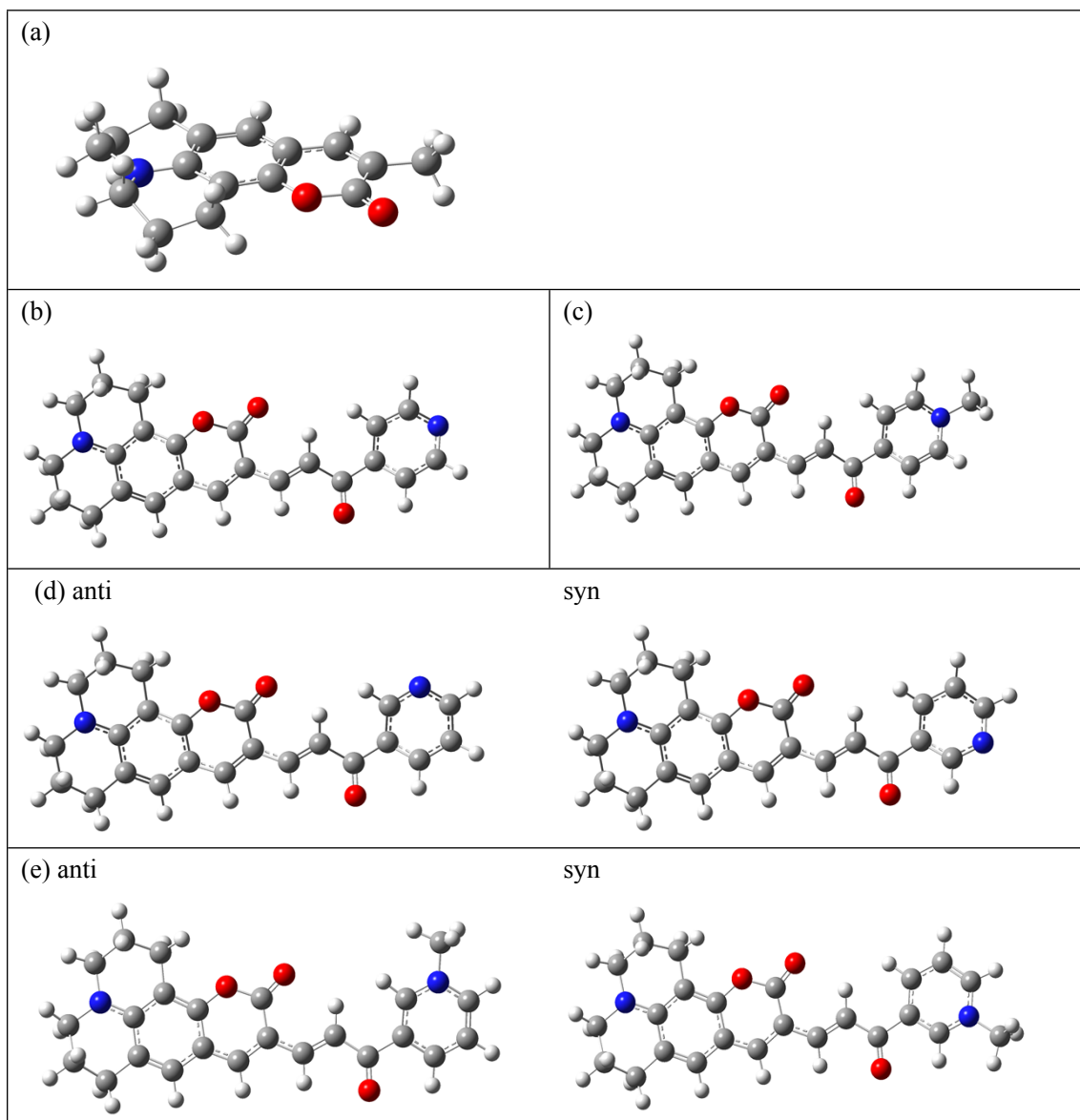


**Fig. S14.** Computed molecular structures. Selected conformations of (a) model coumarin; (b) **m7**; (c) *p*-PSP; (d) **m6**; (e) *m*-PSP.

The coumarin chromophore was planar except for the chain of methylene groups in the six-membered rings. Two conformations were considered with different orientations of the bridges. The energy difference turned out to be insignificant, and the structure shown in Figure S11(a) was adopted in the subsequent calculations of more complex molecules.

For the extended coumarin, *s*-cis and *s*-trans conformers about the coumarine-C=C and the C=C-C=O bond are possible. The 4-substituted pyridine (**m7**) and the *N*-methyl pyridinium ion (*p*-PSP) revealed a preference for the conformations shown in figure S11(b) and (c). Not unexpectedly, other conformations exist with only slightly higher energies, but we restricted our calculations to

the conformations shown. For the meta-substituted pyridine and pyridinium ions *m*-PSP and **m6**, two different orientations of the pyridine ring with respect to the carbonyl group are possible. The anti-conformation is marginally lower in energy in the neutral pyridine **m6**, but slightly higher in energy in the pyridinium ion *m*-PSP (Figure S11(d,e)).

**Table S1.** Energies and excitation energies of selected conformers.

compound	energy <sup>a</sup>	Excitation energies <sup>b</sup> and oscillator strengths					
		B3LYP <sup>c</sup>		CAM-B3LYP <sup>c</sup>		PBE0 <sup>c</sup>	
coumarin	-825.18903	3.260	0.507	3.630	0.652	3.364	0.545
m7	-1223.70546	2.584	1.110	3.014	1.455		
m6 anti	-1223.70645	2.542	1.180	2.957	1.501	2.643	1.275
m6 syn	-1223.70627	2.555	1.180	2.962	1.497	2.654	1.276
<i>p</i> -PSP	-1263.46639	1.942	0.635	2.656	1.322	2.083	0.724
<i>m</i> -PSP anti	-1263.46604	2.181	0.726	2.801	1.472	2.329	0.888
<i>m</i> -PSP syn	-1263.46670	2.237	0.621	2.808	1.499	2.382	0.871
<i>p</i> -PSP-SO <sub>3</sub> <sup>d</sup>	-1888.04022	1.562	0.031	3.037	0.080	1.798	0.032
<i>m</i> -PSP-SO <sub>3</sub> <sup>d</sup>	-1888.04272	2.087	0.002	3.491	0.802	2.351	0.002
<i>p</i> -PSP-SH <sup>d</sup>	-1662.86414	1.552	0.005	3.214	0.027	1.814	0.005
<i>m</i> -PSP-SH <sup>d</sup>	-1662.86508	1.963	0.003	3.478	0.796	2.236	0.003

<sup>a</sup> B3LYP/6-31G(d)/PCM(water) energy in atomic units

<sup>b</sup> transition from ground state to lowest excited state, in eV

<sup>c</sup> 6-31+G(d) basis set, PCM(water)

<sup>d</sup> data are given for the lowest energy conformer only

For the sulfite and sulfide addition products, a set of ~30 low-energy conformations was generated using semi-empirical AM1 calculations in Spartan08. These were then minimized using the B3LYP/6-31G(d)/PCM(water) method in Gaussian09. The conformers that were > 2 kcal/mol higher in energy than the global minimum were not studied further. An exhaustive exploration of the conformational space is prohibited by the computational demands, but the set of conformations obtained in this way should give a representative picture.

For the sulfide adduct *p*-PSP-SH, seven conformers were obtained. For the sulfite adduct *p*-PSP-SO<sub>3</sub> only four low-energy conformers were found. The adducts *m*-PSP-SH and *m*-PSP-SO<sub>3</sub> have more conformational flexibility, and ten conformers were found within 2 kcal/mol of the global minimum in both cases.

Excitation energies and oscillator strengths were calculated using the 6-31+G(d) basis set, with the PCM for water, and three different functionals:

- (a) B3LYP, which is one of the most commonly used functionals for general use

- (b) CAM-B3LYP, a functional designed to counteract the known deficiency of DFT methods to prefer delocalization of electrons, and to incorrectly favor charge-separated states.<sup>2</sup>
- (c) PBE0, a popular functional for excited state calculations<sup>3</sup>

### Predicted absorption energies

The computed excitation energies at the ground state optimized structures should correspond closely to the maxima in the experimental absorption spectra. For the coumarin model, the excitation energies (~420 nm, ~2.95 eV) are overestimated with all three functionals, B3LYP being the closest to experiment. For **m6** (511 nm, 2.43 eV) the red shift relative to the coumarin is qualitatively correctly predicted, but overestimated.

The absorption maxima of *m*-PSP (529 nm, 2.34 eV) and *p*-PSP (~550 nm, ~2.25 eV) are further red shifted. Indeed, shifts to lower energy are predicted using all three functionals. The PBE0 and B3LYP functionals drastically overestimate the red shift. These results are in agreement with the well-known deficiencies of DFT methods in describing delocalization and charge transfer. Especially the B3LYP method underestimates the excitation energy, and PBE0 performs only marginally better. CAM-B3LYP was designed to overcome this type of error.<sup>2</sup> It predicts the red shifts upon extending conjugation and extent of charge transfer much more accurately than the other functionals, but it consistently predicts too high excitation energies.

For the sulfide and sulfite adducts, the results are complicated due to the presence of multiple low-energy conformations. Experimentally, the lowest energy absorption and emission indicate that the nature of the lowest excited state in *m*-PSP adducts is coumarin-localized. The B3LYP and PBE0 calculations of the absorption energies of the sulfide adduct *m*-PSP-SH, however, indicate that there are at least two charge-transfer states at lower energies than the coumarin transitions. This disagreement with experiment can be attributed to the well-known problems that DFT functionals have with charge delocalization. The CAM-B3LYP functional, on the other hand, predicts coumarin-localized excited states to be the lowest in almost all conformations of *m*-PSP-SH. In 4 of the 10 investigated conformers, the second excited state, however, is < 0.2 eV higher in energy, and quite strongly mixed with the coumarin locally excited state.

We next consider the orbitals involved in the low-energy absorptions of *m*-PSP-SH (as an example) using the CAM-B3LYP results. The HOMO in all cases is localized on the coumarin chromophore. The LUMO and LUMO+1 are on the pyridinium unit, and only the next MO, LUMO+2 is on the coumarin. Despite this, the strongly allowed transition to the coumarin locally excited state (HOMO → LUMO+2 mixed with a little HOMO → LUMO contribution) is the lowest in energy. The second excited state (with low oscillator strength) is composed of the same configurations, but with strongly predominant HOMO → LUMO character.

The relevant MO's are shown in Figure S12. The Kohn-Sham orbitals calculated with the B3LYP and PBE0 functionals are similar to the ones shown in Figure S12, but the CT states (HOMO → LUMO and HOMO → LUMO+1) are predicted to be lower in energy.

For the second conformer of *m*-PSP-SH, only 0.01 kcal/mol above the lowest energy one, the orbitals are very similar, but the lowest excited states have mixed character, consisting of linear combinations of the CT configuration and the LE configuration.

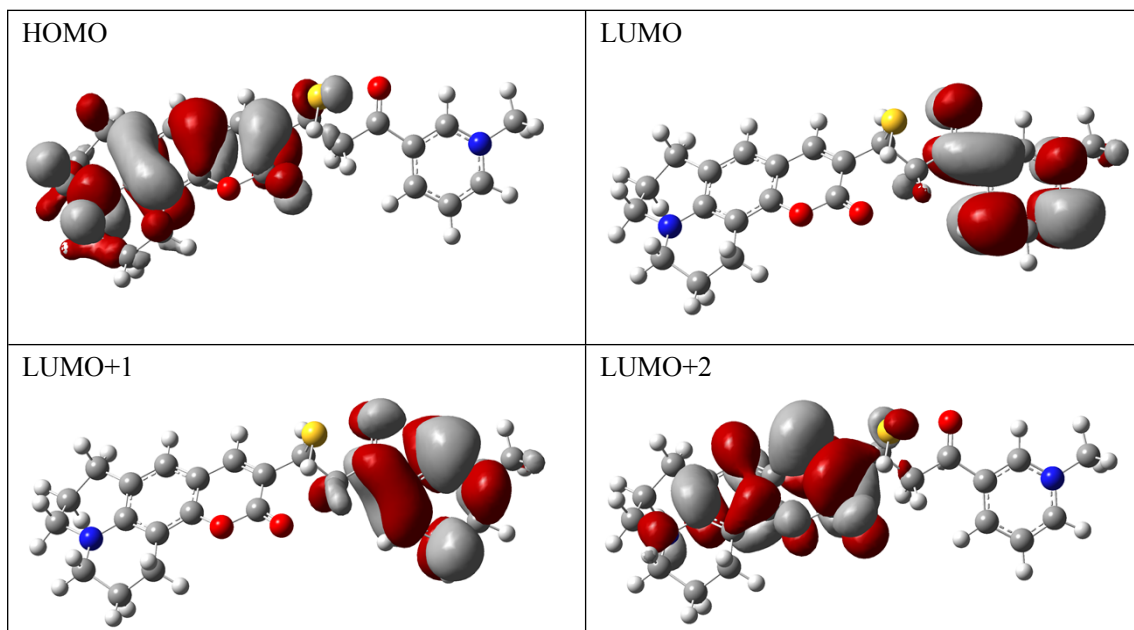


**Figure S15.** Frontier orbitals of the lowest-energy conformer of *m*-PSP-SH calculated at the CAM-B3LYP/6-31+G(d) level.

TDDFT calculations were run on the seven lowest-energy conformers of *p*-PSP-SH. In this case, the lowest energy transitions were predicted to be to charge-transfer states for all conformers considered, even with the CAM-B3LYP functional. For *p*-PSP-SO<sub>3</sub>, four low-energy conformers were found. In all of these, even with CAM-B3LYP, the charge-transfer transition was favored. In Table S1 we only give the lowest energy transition. The coumarin-located excitation is strongly allowed and easily recognized in Table S1 by its high oscillator strength.

## Conclusion

The calculations predict the changes in the absorption spectra going from the coumarin to **m6**, and *m*-PSP and *p*-PSP fairly well. For the adducts of sulfite and sulfide to *m*-PSP and *p*-PSP, B3LYP/6-31+G(d) and PBE0/6-31G+g(d) calculations predict charge-transfer transitions at clearly lower energy than the absorption of the coumarin chromophore. Only the CAM-B3LYP functional predicts coumarin transitions at the lowest energy for *m*-PSP-SH and *m*-PSP-SO<sub>3</sub>. Charge transfer transitions are, however, found at only slightly higher energies, and in some conformers of *m*-PSP-SH and *m*-PSP-SO<sub>3</sub> are mixed with the coumarin transitions. For *p*-PSP adducts, CT transition were predicted to be the lowest energy ones, even with CAM-B3LYP. Presumably, the low-energy charge transfer states provide the excited state relaxation channels that lead to relatively rapid nonradiative decay. This explains why the quantum yields of fluorescence of the adducts are low, even though they are larger than those of *m*-PSP and *p*-PSP.

## References

1. Gaussian09, Rev. A.02, M. J. Frisch, G. W. Trucks, H. B. Schlegel, G. E. Scuseria, M. A. Robb, J. R. Cheeseman, G. Scalmani, V. Barone, B. Mennucci, G. A. Petersson, H. Nakatsuji, M. Caricato, X. Li, H. P. Hratchian, A. F. Izmaylov, J. Bloino, G. Zheng, J. L. Sonnenberg, M. Hada, M. Ehara, K. Toyota, R. Fukuda, J. Hasegawa, M. Ishida, T. Nakajima, Y. Honda, O. Kitao, H.

- Nakai, T. Vreven, J. A. Montgomery, J. E. Peralta, F. Ogliaro, M. J. Bearpark, J. J. Heyd, E. Brothers, K. N. Kudin, V. N. Staroverov, R. Kobayashi, J. Normand, K. Raghavachari, A. Rendell, J. C. Burant, S. S. Iyengar, J. Tomasi, M. Cossi, N. Rega, J. M. Millam, M. Klene, J. E. Knox, J. B. Cross, V. Bakken, C. Adamo, J. Jaramillo, R. Gomperts, R. E. Stratmann, O. Yazyev, A. J. Austin, R. Cammi, C. Pomelli, J. W. Ochterski, R. L. Martin, K. Morokuma, V. G. Zakrzewski, G. A. Voth, P. Salvador, J. J. Dannenberg, S. Dapprich, A. D. Daniels, O. Farkas, J. B. Foresman, J. V. Ortiz, J. Cioslowski, D. J. Fox, Gaussian Inc., Wallington CT, **2009**.
2. T. Yanai, D. P. Tew, N. C. Handy, *Chem. Phys. Lett.* **2004**, *393*, 51–57.
  3. D. Jacquemin, E. A. Perpète, G. E. Scuseria, I. Ciofini, C. Adamo, *J. Chem. Theory Comput.* **2012**, *4*, 123–135.